Environmental Earth Sciences (2025) 84:373
https://doi.org/10.1007/s12665-025-12172-w

ORIGINAL ARTICLE

Modifying of turbulent kinetic energy constants: a comparison among shear stress methods in compound meandering channels

Vahideh Mortazavi Amiri[1] · **Kazem Esmaili**[1]

Received: 2 August 2024 / Accepted: 28 February 2025

Abstract
Understanding the intricate dynamics of flow and sediment transport within compound meandering channels is vital for designing stable channels. The interplay of centrifugal forces, hydrostatic pressure, and shear stress significantly influences the complex flow patterns in these channels. Shear stress serves as a pivotal parameter for predicting bank erosion and bend migration, influenced by local accelerations, decelerations, and secondary flows. Momentum transfer between the primary channel and adjacent floodplains intricately shapes shear stress distribution in various sections. This study involves an analysis of laboratory data focusing on meandering channel patterns and the forces acting on their boundaries in the intricate three-dimensional flow within bends. Four methods—linear regression (LR) of flow velocity profiles, turbulent kinetic energy (TKE), modified turbulent kinetic energy (TKE-w′), and Reynolds shear stress extrapolation (RSS)—were employed based on ADV data collected in a compound meandering channel. The research aims to validate modified TKE and TKE-w′ constants, which demonstrated improved accuracy compared to conventional constants. Additionally, the study discusses the position of maximum shear stress in these channels, shedding light on their critical locations.

Keywords Compound meandering channels · Reynolds shear stress · Turbulent kinetic energy (TKE) · Modified turbulent kinetic energy (TKE-w′)

Introduction

A significant proportion of rivers exhibit meandering patterns, often accompanied by one or more floodplains. During high-flow events that exceed the channel's capacity, these floodplains function as conveyance zones, accommodating the surplus discharge. Under such conditions, the flow structure undergoes considerable alteration due to the complex momentum exchange between the high-velocity flow in the main channel and the low-velocity flow in the floodplains (Fukuoka and Uchida 2014). This interaction leads to the formation of shear layers and turbulence induced by the channel geometry. Additionally, the combined effects of centrifugal and pressure-driven forces, along with Reynolds stresses, contribute to the development of vortical structures within the turbulent flow.

The accuracy of flow predictions in compound channels is significantly influenced by secondary flows and turbulence anisotropy. Shan et al. (2015) proposed an analytical model for predicting depth-averaged velocity in smooth compound meandering channels based on experimental data. However, the highly three-dimensional nature of flows in such channels presents a persistent challenge for river management research (Mera et al. 2015). Recent investigations have increasingly focused on unravelling the complex flow dynamics in meandering compound channels (Chen et al. 2018; Esfahani and Keshavarzi 2020; Hafez 2022; Naghavi et al. 2023). Pan et al. (2019) explored velocity distribution characteristics and flow discharge capacity within a physical meandering channel featuring one-sided vegetated floodplains.

Despite advancements, accurately predicting flow patterns in meandering rivers remains a challenging task due to the inherent hydrodynamic complexities. Blanckaert (2011) examined three critical hydrodynamic processes in meandering rivers—secondary flow saturation, outer-bank cells, and

✉ Kazem Esmaili
esmaili@um.ac.ir

Vahideh Mortazavi Amiri
v.mortazavi@um.ac.ir

[1] Department of Water Science and Engineering, Ferdowsi University of Mashhad, Mashhad 9177948974, Iran

Published online: 21 June 2025

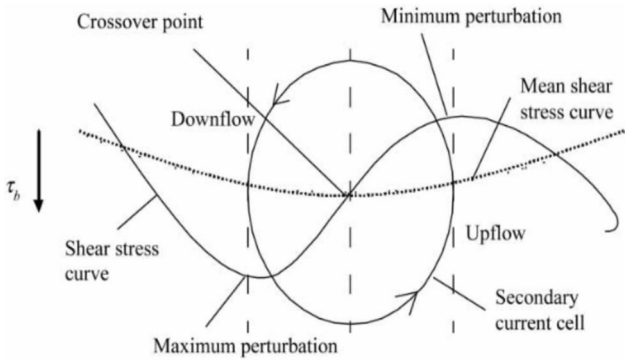

Fig. 1 Effect of secondary current cell on boundary shear stress (Omran and Knight 2010)

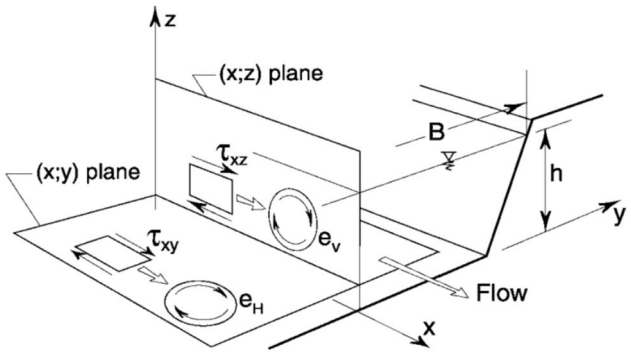

Fig. 2 Vertical and horizontal planes of rotation of CS's (Da Silva 2006)

inner-bank flow separation—all of which significantly affect shear stress in these channels. Given its critical role in sediment dynamics, shear stress warrants detailed investigation, particularly regarding its influence on erosion processes in meandering rivers. The magnitude and spatial distribution of shear stress are pivotal in shaping sediment transport and deposition patterns. Therefore, accurately predicting shear stress distributions within meandering compound channels is essential for effective river management.

Figure 1 illustrates the impact of secondary current cells on turbulence and boundary shear stress distributions. The integration of secondary flow parameters is, therefore, crucial for precise calculations and modeling of shear stress in meandering compound channels. Parsapour-Moghaddam and Rennie (2017), employing the Delft-3D hydrostatic model for a meandering river reach, demonstrated that the model could reliably predict the location and magnitude of secondary flow cells. Their findings showed good agreement with field velocity profiles, further underscoring the importance of incorporating secondary flow dynamics in shear stress analysis.

A substantial body of research has investigated shear stress distribution in both straight and compound channels. Mignot et al. (2009) investigated shear stress in a rough bed experimental channel. Zarrati et al (2008) determined the distribution of shear stress in straight and compound channels based on Reynolds stresses and the effect of the shear layer produced by secondary flows between the main channel and floodplains. Coherent structures (CS) shown in Fig. 2 illustrate turbulent eddies that can evolve as vertical components in (x, z) planes or horizontal components in (x, y) planes. Guo and Julien (2005) used an analytical solution for the determination of mean shear stress in smooth open channel flow. Ippen et al. (1960) and Ippen and Drinker (1962) conducted experimental tests and found that high values of shear stress in curves could be observed near the inner and outer banks and before the curve exit. Yang and Woo (2007) determined the shear stress distribution in an experimental gradually varied flow. They established that a zero wall-normal velocity condition implies a linear distribution of Reynolds shear stress.

Several established methods, including linear regression (LR) of flow velocity profiles, turbulent kinetic energy (TKE) analysis, and Reynolds shear stress (RSS) extrapolation, have been employed by researchers to determine shear stress distributions within compound channels (Bernard and Handler 1990; Hooke 1975; Noorbakhsh and Parola 2018; Jing et al. 2009). Alfadhli et al. (2013) investigated the Reynolds shear stress distribution in steady and unsteady flows. They pointed out that flow acceleration and velocity increase or decrease could have a significant effect on Reynolds shear stress distribution. Hopkinson and Wynn-Thompson (2012) investigated the applicability of the Turbulent Kinetic Energy (TKE) method for calculating bed shear stress in compound channels with turbulent flow generation. Their analysis included a comparison between the TKE method and experimental data, highlighting the need to examine the variability of the C coefficient within the TKE equation for this specific channel geometry. Prior research suggests significant spatial variability in the constant values used within the Turbulent Kinetic Energy (TKE) equation for fluvial environments (Biron et al. 2004). Zhang et al. (2020) proposed modified constants specifically for the TKE-w' and TKE equations to address this challenge.

Building on the established importance of shear stress, a thorough understanding of its influence on sediment transport mechanisms remains critical for effective river management strategies. This study investigates the applicability of various bed shear stress calculation methods utilizing Acoustic Doppler Velocimetry (ADV) velocity data within the context of meandering compound channels. A comparative analysis will be conducted to assess the performance of these methods in this specific fluvial environment. The applicability of certain investigated methods to complex channel geometries and three-dimensional flow characteristics may

necessitate adaptations. While traditional methods of shear stress estimation, are widely used for straight and regular channels, they do not adequately capture the complex flow dynamics that occur in meandering channels. The proposed new constant provides a correction factor that accounts for the influence of channel curvature, sinuosity, and the resulting secondary flow structures on shear stress distribution.

Experimental setup

The present experiments were carried out in a rectangular channel at the physical hydraulic model's laboratory of department of Ferdowsi University of Mashhad, Mashhad, Iran. The model was 1.2 m wide, 20 m long, and 0.7 m high channel flume set at a fixed slope of 0.0002. A rock-filled box was placed at the inlet to reduce turbulence and ensure the flow entered with parallel streamlines. The flow depth was 15 cm in the main channel and 10 cm in the floodplains. Table 1 lists the geometrical features of the experimental channel. Experiments were conducted over a fixed bed and a series of meanders including three curves, was constructed in the experimental channel. The physical model was designed to replicate the characteristics of meandering rivers, with a focus on the sinuosity parameter as a fundamental criterion. The sinuosity index, defined as the ratio of the channel's thalweg length to the valley length, is a key descriptor of meandering rivers. For meandering channels, a minimum sinuosity index of 1.5 is generally required to classify the channel as meandering. This threshold served as the basis for the design of the experimental bends. To ensure the physical model fit within the constraints of the experimental facility, specifically the flume width of 120 cm, the channel geometry was carefully designed. The curvature and shapes of the bends were iteratively adjusted to achieve the desired sinuosity while staying within the spatial limits of the flume. The resulting design produced a channel with well-defined meanders, maintaining a representative flow path and cross-sectional area that mimic natural meandering rivers. Once the design was finalized, the meandering main channel was constructed in the flume using durable materials to ensure stability during experimentation. Special attention was given to the transitions between bends and straight segments to accurately replicate the flow characteristics of natural systems. The total flow rate was 22.3 L per second, supplied by a recirculation water system. The constant depth of 25 cm resulted in a Froude number of 0.2 (Table 2).

Three-dimensional velocity measurements obtained using a 25 Hz frequency Nortek Down-looking Acoustic Doppler Velocimeter (ADV) at five longitudinal locations (cross-sections CS_1–CS_5) at different water depths. This setup allowed for the measurement of velocity in three dimensions. Time series stationary data were collected at two points along the developed flow section, at both the mid-depth and near-bed locations of the channel. For each of these measurement points, velocity time series were recorded for a duration of 600 s. As shown in Fig. 2, the velocity time series demonstrated stable flow conditions after 100 s, and this stabilization period was considered the appropriate duration for data collection at the specified grid points. The velocity data were initially recorded using the Vectrino software. Afterward, the data underwent post-processing using the WinADV software. The post-processing steps included filtering the data based on a minimum correlation threshold of 70% and a minimum signal-to-noise ratio (SNR) greater than 15 (Barahimi and Sui 2024). Additionally, we applied the Phase-Space Threshold Despiking statistical model to remove any outlier or spurious velocity values, ensuring the accuracy and reliability of the dataset for subsequent analysis. Figure 3 illustrates the Schematic geometry of the physical model and Image of the ADV system. Figure 4 presents the two-dimensional distribution of detailed velocity measurement points within the channel's cross-sections.

In this study, channel sinuosity is a key geometric parameter that measures the degree of meandering in a river or channel. It is calculated as the ratio of the channel's thalweg length (the deepest path of the channel) to the straight-line distance between its endpoints. For the physical model used in this research, the thalweg length is 1.75 m, and the straight-line distance is 1 m. Therefore, the channel's sinuosity is 1.75, indicating a moderately sinuous channel, which aligns with the design of the physical model.

Table 1 Details of physical model geometry

No.	Item description	Experimental channel
1	Channel type	Meander
2	Geometry of main channel section	Rectangular
3	Geometry of flood plain section	Rectangular
4	Flood plain type	Asymmetric
5	Flood plain width (B)	0.05–0.95 m
6	Main channel base width (b)	0.2 m
7	Depth of main channel (H)	0.15 m
8	Bed slope of the channel	0.0002
9	Sinuosity	1.75

Table 2 Experimental parameter values

Q (m^3/s)	Fr	R_c/b	H (cm)
0.0583	0.42	2.75	15

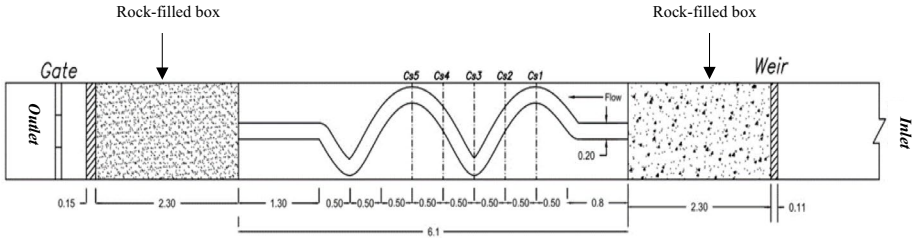

(a)

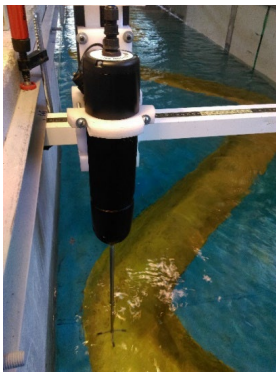

(b)

Fig. 3 **a** Schematic plan view of meandering compound channel (Dash lines show measured cross sections), **b** Image of ADV system

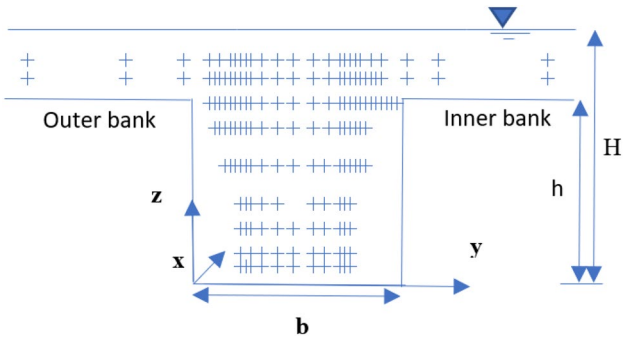

Fig. 4 Measured velocity points at section Cs_4 in the meandering channel

Quadrant analysis and bursting events

The primary objective of analyzing three-dimensional bursting events within turbulent flow structures, influenced by centrifugal forces and a free surface, is to determine the direction of particle motion within the fluid (Keshavarzi and Gheisi 2006; Esfahani and Keshavarzi 2011). The analysis of burst event in the bed of meandering channels aids in identifying regions with a high potential for erosion. Therefore, for the application of this method in the present study, two-dimensional velocity data were utilized at five cross-sections containing bends. The bursting process is categorized into four types of turbulent events: sweeps, ejections, outward interactions, and inward interactions, based on the signs of velocity fluctuations u′ and w′. In the present study, this method was applied using two-dimensional velocity data at five cross-sections containing bends. The bursting process is classified into four types of turbulent events—sweeps, ejections, outward interactions, and inward interactions—based on the signs of velocity fluctuations (u′ and w′). These fluctuations are calculated relative to the time-averaged velocities in the longitudinal (uuu) and vertical (www) directions, providing insights into the dynamic mechanisms of momentum and sediment exchange within the flow.

The four quadrants are defined as follows:

- The first quadrant (Q1: $u' > 0$, $w' > 0$) represents outward interactions.
- The second quadrant (Q2: $u' < 0$, $w' > 0$) corresponds to ejections, characterized by the upward movement of low-velocity fluid, which transports already-entrained sediments into the flow.
- The third quadrant (Q3: $u' < 0$, $w' < 0$) describes inward interactions.
- The fourth quadrant (Q4: $u' > 0$, $w' < 0$) represents sweeps, which facilitate the entrainment of sediments into the flow (Bauri and Sarkar 2018).

Shear stress calculation methods

The interaction between floodplain and main channel flows, combined with the sinuous morphology of meandering rivers, generates secondary currents and facilitates momentum transfer across the floodplain-main channel interface. This interaction creates complex flow conditions, making the determination of shear stress near the riverbed and within various water depth layers particularly challenging. Several methods have been proposed for estimating shear stress in open channels, including Linear Regression (LR), Turbulent Kinetic Energy (TKE), modified Turbulent Kinetic Energy (TKE-w′), and Reynolds Shear Stress Extrapolation (RSS). These approaches have proven to be effective under specific conditions; however, further evaluation and validation are necessary to ensure their accuracy and applicability under diverse hydraulic scenarios.

Linear Regression (LR) of the longitudinal velocity profile

The most popular method in river process studies is the reach-averaged bed shear stress (Babaeyan-Koopaei et al. 2002). It is defined as:

$$\tau_0 = \rho g R S_f \tag{1}$$

where τ_0 is bed shear stress, ρ is water density, g is the acceleration due to gravity, R is hydraulic radius and S_f is the energy slope. However, this method is not appropriate for local, small-scale estimates of the variations in shear stress.

Based on the relationship between the logarithmic profile of flow velocity versus the depth, a linear regression of flow velocity profile for shear stress calculation is applied (sin 2010; Imagbe 2021).

$$u = \frac{u_*}{\kappa} ln \frac{z}{z_0} \tag{2}$$

$$u = \frac{u_*}{\kappa} ln\, z + c \tag{3}$$

where C is a constant equal to

$$\frac{u_*}{\kappa} ln(z_0) \tag{4}$$

$\frac{u_*}{\kappa}$ is the slope of linear regression equation in logarithmic scale and u_* is shear velocity (LT^{-1}), κ is von Karman coefficient (0.4); and z = height above the bottom of channel (L),

As a result, the shear stress can be computed by:

$$\tau = \rho(\kappa S)^2 \tag{5}$$

where S = slope of Eq. (3).

Turbulent kinetic energy (TKE)

Among the established methods for estimating shear stress in open channels, Turbulent Kinetic Energy (TKE) analysis plays a prominent role (Hopkinson and Wynn-Thompson 2012). In this method, three fluctuation velocity components are applied.

$$\tau_0 = C_1 \left[0.5\rho(\overline{u'^2} + \overline{v'^2} + \overline{w'^2})\right] \tag{6}$$

where τ_0 = boundary shear stress, C = proportionality constant (reported between 0.18 and 0.2 (Soulsby 1983), Stapleton and Huntley 1995), ρ = mass density, u' = velocity fluctuations in the downstream direction, v' = velocity fluctuations in the transverse direction; and w' = velocity fluctuations in the vertical direction. The Turbulent Kinetic Energy (TKE) method distinguishes itself by explicitly incorporating flow turbulence. Kim et al. (2000) proposed a modified TKE method (TKE-w') that capitalizes on the inherently lower noise levels observed in vertical velocity fluctuations compared to horizontal ones.

$$\tau_0 = C_2 \rho \left[(\overline{w'^2})\right] \tag{7}$$

where C_2 = 0.9. In the case of bends, modified C_1 = 0.23 and C_2 = 0.44 adopted to calculate the shear stress using TKE and TKE-w′ respectively (Zhang et al. 2020).

Reynolds stress model (RSM)

In complex flows, such as flow in compound meandering channels, the RSM is used to consider vorticity, curvature, and circulation effect on shear stress. In this method, the Reynolds averaged Navie-Stokes equations are solved using Reynolds Stress transport equation and the transport equation of kinetic energy's dissipation rate (Jing, et al 2009). Wahl (2000) presented Eqs. (8) through (13) as shear stress extrapolation method using ADV data.

$$\tau_{xy} = \tau_{yx} = -\rho \times (\text{COV-XY}) \tag{8}$$

$$\text{COV} - \text{XY} = \frac{\sum V_x V_y}{n-1} - \frac{\sum V_x \sum V_y}{n(n-1)} \tag{9}$$

$$\tau_{zx} = \tau_{xz} = -\rho \times (\text{COV-XZ}) \tag{10}$$

$$\text{COV-XZ} = \frac{\sum V_z V_x}{n-1} - \frac{\sum V_z \sum V_x}{n(n-1)} \tag{11}$$

$$\tau_{zy} = \tau_{yz} = -\rho \times (\text{COV - YZ}) \tag{12}$$

$$\text{COV-ZY} = \frac{\sum V_y V_z}{n-1} - \frac{\sum V_y \sum V_z}{n(n-1)} \quad (13)$$

where τ_{xy}, τ_{yx} and τ_{xz} are turbulent shear stress along the y-axis caused by flow velocity fluctuations along the x-axis, turbulent shear stress along the x-axis and caused by flow velocity fluctuations along the y-axis and turbulent shear stress along the z-axis and caused by flow velocity fluctuations along the x-axis ($ML^{-1}\ T^{-2}$) respectively; ρ = mass density (ML^{-3}); and COV-XY = covariance of two variables calculated using Eq. (9). Where V_x and Vy = flow velocity along the x and y-axis (LT^{-1}); and n = number of samples (collected velocity data) (dimensionless) and COV-XZ = covariance of two variables calculated using Eq. (11) Where V_z = flow velocity along the z-axis (LT^{-1}) and COV-ZY = covariance of two variables calculated using Eq. (13).

In this research, a MATLAB code is utilized to generate graphical representations.

Results and discussion

Longitudinal velocity distribution

The variations in boundary shear stress are caused by the combination of velocity vectors in the stream-wise direction and transverse vectors resulting from secondary circulation (Ursic 2012). Figure 5 displays the stream-wise velocity components (u) in the main channel for sections CS_1, CS_3, and CS_5. In section CS_1, velocities near the walls have greater quantities and fluctuations than the other side of the main channel. The same can be observed in the velocity profiles of section CS_5. The sidewall effect caused a decrease in velocity fluctuations in CS_3 and developed flow in a straight main channel toward bending apex. By combining angular flow in floodplains, as can be seen, velocity quantities showed more fluctuation especially in the momentum exchange area (h = 12.5–18.5 cm). Also, the maximum values of stream-wise velocity components occur at CS_1 compared to that with CS_3 and CS_5. The greater values in section CS_1 are due to the less resistance of straight channel flow before entering the curve segment. Additionally, in sections, CS_1 and CS_3 the Maximum R^2 in longitudinal

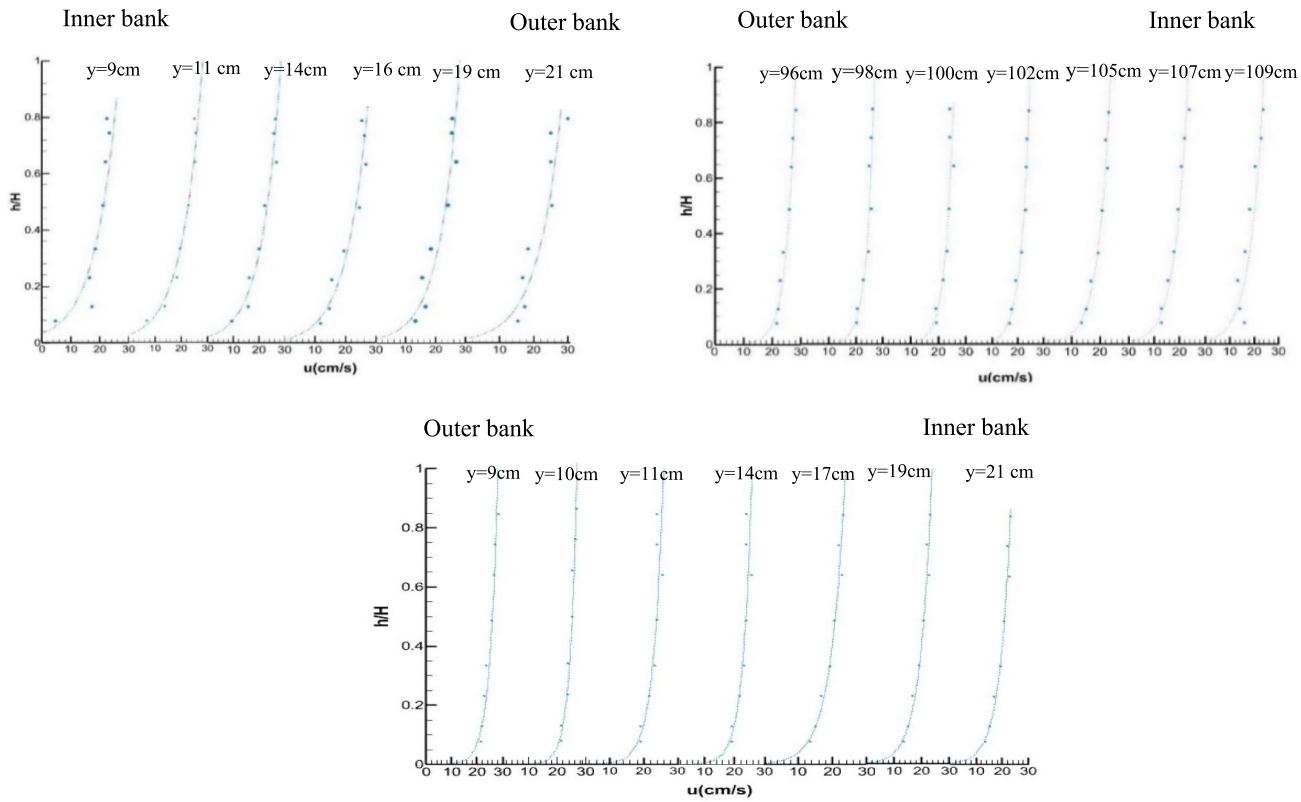

Fig. 5 Cross-sectional stream-wise distribution of velocity component (u)in depth in the main channel (**a**) section CS_1 (**b**) section CS_3 (**c**) section CS_5

velocity profiles can be seen near the middle part of the concave bank.

Secondary cells in compound channels

Secondary cells in meandering compound channels play a vital role in shaping the distribution of shear stress across the main channel and floodplain. These circulations arise from the interplay between centrifugal forces and lateral shear caused by the channel's curvature. They help redistribute momentum and enhance mixing across the channel, leading to variations in shear stress that directly affect sediment transport processes, such as erosion and deposition. In areas with strong secondary flows, higher shear stress is typically observed along the outer banks of bends, accelerating sediment entrainment and contributing to bank erosion. In contrast, lower shear stress along the inner banks creates favorable conditions for sediment deposition. The interaction between the main channel and the floodplain, driven by these circulations, forms lateral shear zones that can destabilize banks or facilitate sediment exchange. These secondary flows play a crucial role in influencing channel morphology and sediment dynamics, making them essential for understanding how meandering channels evolve. Figure 6 secondary flow structures at cross-sections CS1–CS5. In all cross-sections, the rotation direction of the central region cells is opposite to that of the cells near the banks, With the exception of C4.

Quadrant analysis

Figure 7 illustrates the distribution of turbulent fluctuations in the u′–w′ plane. The quadrant analysis results clearly demonstrate the spatial distribution of turbulent bursting events, highlighting their roles in momentum and sediment exchange processes within the channel.

These fluctuations are calculated relative to the time-averaged velocities in the longitudinal (u) and vertical (w) directions that provide insights into the dynamic mechanisms of momentum and sediment exchange in the flow. The first quadrant (Q1), where $u' > 0$, $w' > 0$, represents outward interactions. The second quadrant (Q2), with $u' < 0$, $w' > 0$, corresponds to ejections, characterized by the upward movement of low-velocity fluid, which transports already-entrained sediments into the flow. The third quadrant (Q3), defined by $u' < 0$, $0w' < 0$, describes inward interactions. Finally, the fourth quadrant (Q4), where $u' > 0$, $w' < 0$, represents sweeps, which facilitate the entrainment of sediments into the flow (Bauri and Sarkar 2018).

The quadrant analysis results indicate a clear distribution of turbulent bursting events, represented by fluctuations in the u′–w′ plane.

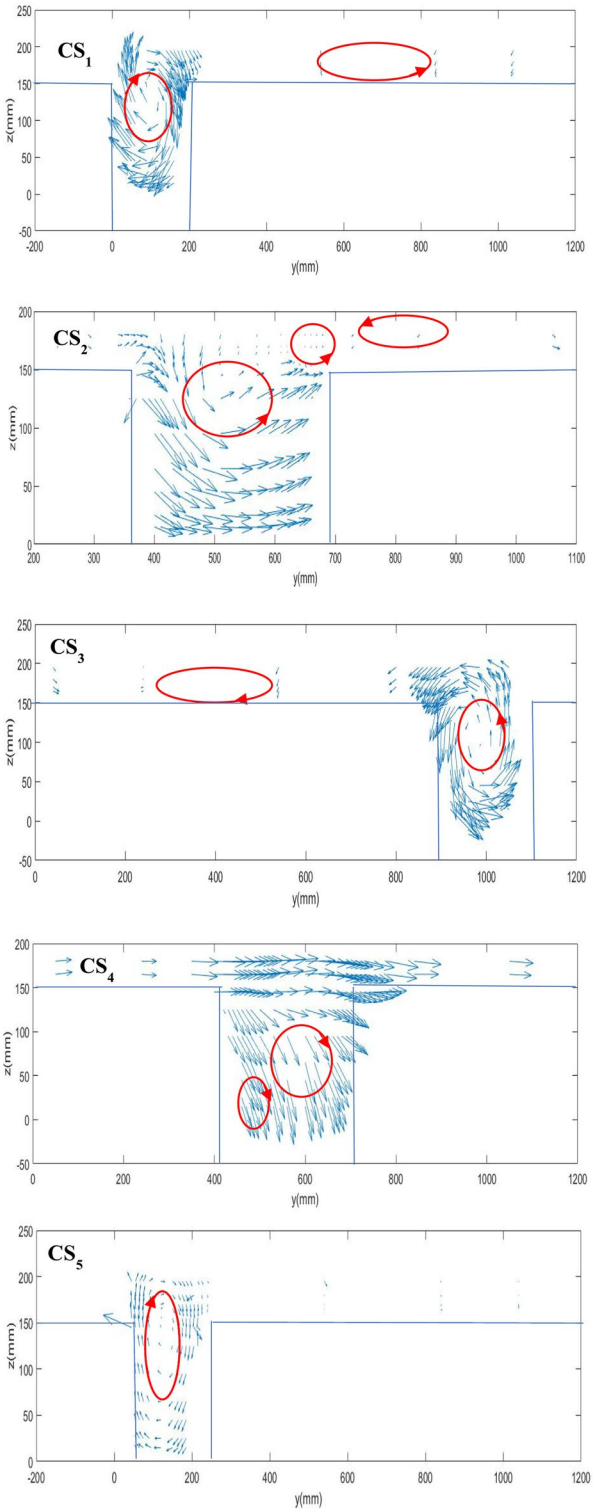

Fig. 6 Secondary flow structures at cross-sections CS1–CS5

1. **Ejection Events (Q2):** The ejection events, dominate the upper-left quadrants of the scatter plots. These events suggest upward motion of low-speed fluid, often linked to the transportation of sediment into the flow.

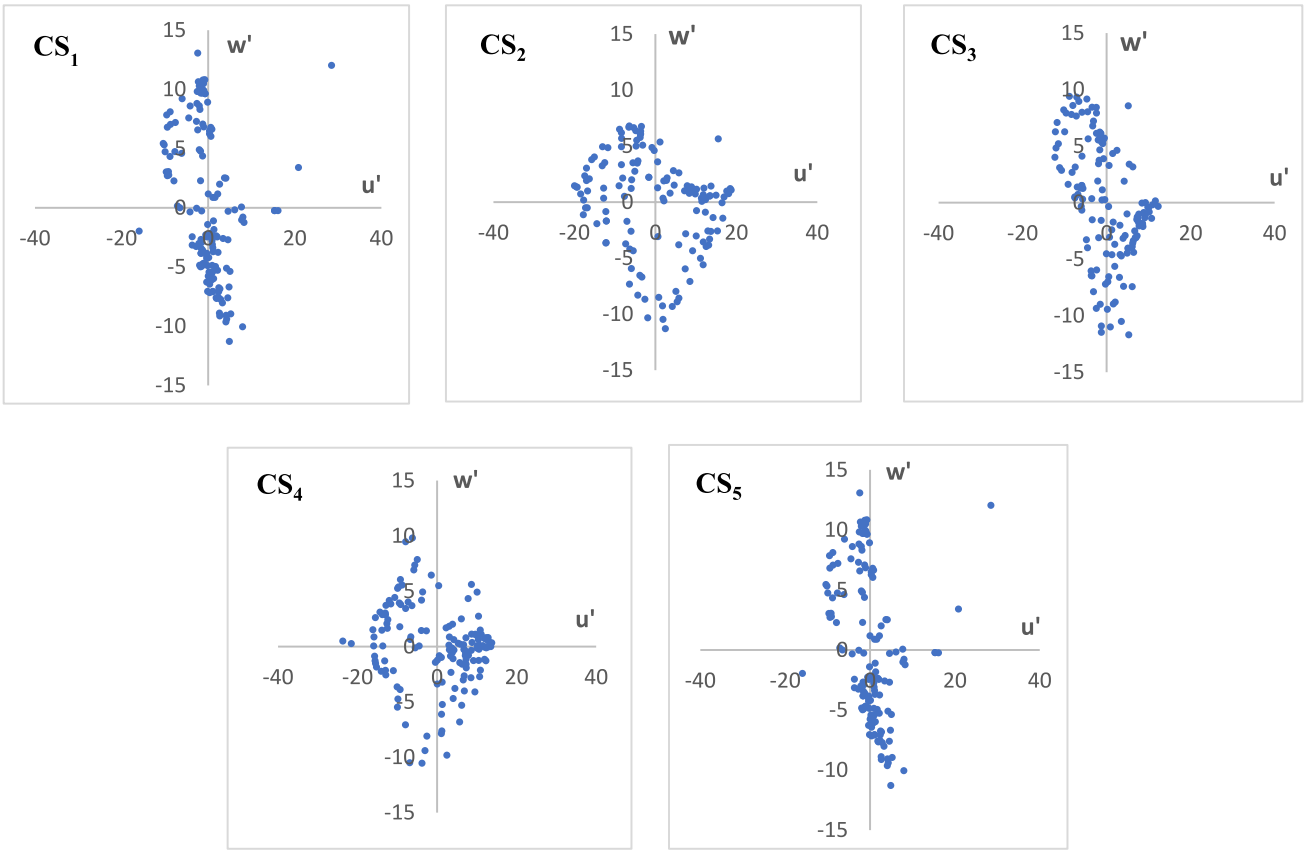

Fig. 7 Variation of longitudinal and vertical velocity fluctuations in the u′–w′ plane

Their prominence reflects the active role of turbulence in entraining sediment, especially in areas of adverse pressure gradients, such as near curved channel beds.

2. **Sweep Events (Q4):** The sweep events dominate the lower-right quadrants. These bursts involve downward movement of high-speed fluid, enhancing the entrainment of sediment from the bed into suspension. The relatively dense concentration of data points in this quadrant highlights the strong role of sweeps in driving bed-sediment interactions.

Outward and inward interactions (Q1 and Q3)

Outward interactions and inward interactions are less frequent compared to ejections and sweeps. Outward interactions are indicative of high-speed fluid moving upward, which may contribute to turbulence in the near-surface regions, while inward interactions represent low-speed downward motions that contribute to turbulence dissipation near the bed. The scatter plots (Fig. 6) reveal an asymmetry between ejections and sweeps, with ejections slightly dominating in magnitude. This imbalance is consistent with prior studies showing that upward transport mechanisms (ejections) often outweigh downward entrainment mechanisms (sweeps) in turbulent flows, particularly in meandering or compound channels with complex secondary flow patterns. The spread of points in each quadrant also indicates the variability and strength of turbulent structures. The larger spread observed in Q2 and Q4 highlights the critical contribution of these events to the exchange of momentum between the bed and overlying flow. These observations align with findings in environmental hydraulics, emphasizing the significant influence of turbulent bursting events on sediment dynamics. The distribution of quadrant events may be further influenced by the geometric properties of the meandering channel, such as sinuosity and bend curvature. These features can amplify secondary flows, causing stronger ejection and sweep dominance at specific locations along the bends. The quadrant analysis reveals that ejection and sweep events are the primary contributors to sediment and momentum exchange in the flow, consistent with the theoretical understanding of turbulent bursting in open-channel flows. These findings provide valuable insights for environmental and hydraulic applications, particularly in the design and management of meandering river systems. The charts (Fig. 8) represent quadrant contributions from various cross-sectional regions of the channel. The quadrant contributions show the percentage of the total flow or other hydrodynamic quantities

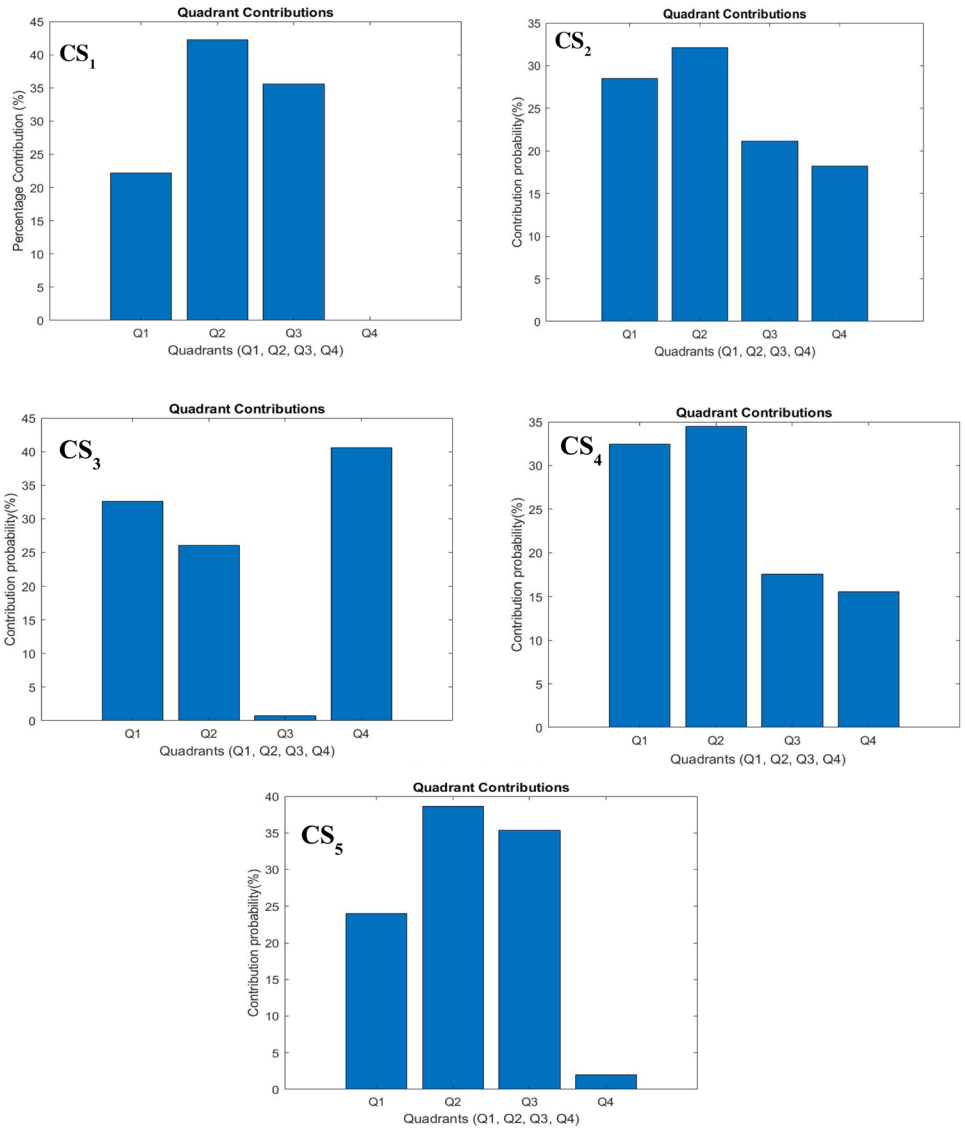

Fig. 8 Contribution probability of events at cross-sections CS1–CS5

distributed across four quadrants (Q1, Q2, Q3, and Q4) for the measurements. Each chart compares the relative distribution of contributions across the quadrants at a cross section, indicating where the major momentum or stress contributions are found. The variation in contributions between the quadrants reflects differences in flow dynamics or turbulence at different points in the channel.

Distributions of Reynolds stress components

Secondary flow cells play a critical role in generating turbulence within the interface regions of compound channels. As a result, Reynolds stress components are particularly effective in simulating shear stress in these systems (Rameshwaran and Nade 2003; Biron et al. 2004). Yang and McCorquodale (2004) demonstrated strong agreement between analytical Reynolds Stress Models (RSM) and experimental data, highlighting the reliability of this approach. In compound channels, the interaction zone near the main channel-floodplain interface is significantly influenced by the shear layer and the vertical gradient of shear stress. These dynamics are closely tied to transverse momentum exchange processes. Vertical profiles of Reynolds shear stress at the main channel for cross-section CS1, as shown in Fig. 9, illustrate these effects. The pronounced fluctuations observed in the center of the cross-section (y = 11 cm) suggest the presence of stronger secondary flows in this region, underscoring their influence on the vertical shear stress distribution.

Structure of shear stress across layer near the bed in the main channel

Figure 10 presents the bed shear stress distributions in the main channel under overbank flow conditions,

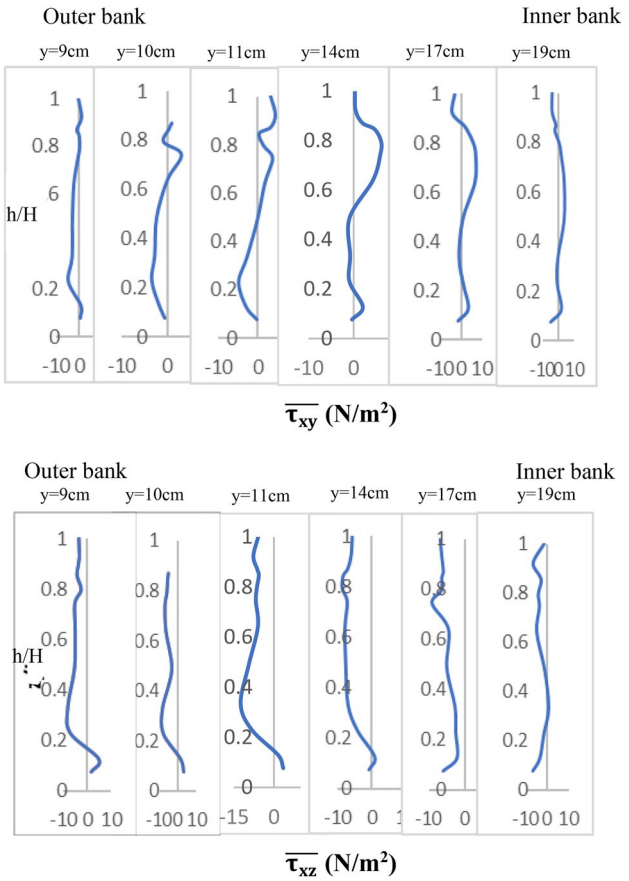

Fig. 9 Distribution of Reynold shear stresses in relative depth at section Cs_1

computed using three previously described methods. The results indicate that the linear regression method consistently predicts lower shear stress values compared to the other approaches. The turbulent kinetic energy (TKE) method, on the other hand, demonstrates a pattern that closely aligns with the Reynolds shear stress extrapolation method, particularly in the bend regions. This similarity likely reflects the dynamic flow characteristics in meandering channels, where shear stress is strongly influenced by Reynolds stresses.

The lower estimates from the linear regression method may stem from its reliance on mean velocity profiles, making it more suitable for fully developed logarithmic flow conditions. In contrast, the TKE and Reynolds shear stress methods consider turbulent velocity components in three flow directions, enabling them to capture the complex turbulence structures in meandering flows more effectively. Notably, all methods exhibit a strong agreement in cross-section CS2, located at the entrance to the bend, highlighting the critical role of this region in shaping bed shear stress distribution in compound channels.

Structure of shear stress across layers of relative water depth in main channel

Figures 11, 12, 13 and 14 illustrate the distribution of Reynolds shear stress at various depths of the channel, from cross-sections CS1 to CS5. In compound channels, anisotropic turbulence arises due to the differing behavior of velocity fluctuations v′ and w′ (Rameshwaran and Pamela 2003). The graphical analysis highlights that at a water depth of 12.5 cm, the Reynolds shear stress exhibits the greatest variation compared to other layers, emphasizing the role of momentum exchange within the interaction region. At this depth, the maximum energy exchange occurs between the main channel and the flood plain, particularly in the surrounding interface zone. Consequently, shear stress reaches its highest levels at these interfaces, underlining the critical role of flow dynamics in sediment transport and channel morphology in compound meandering systems.

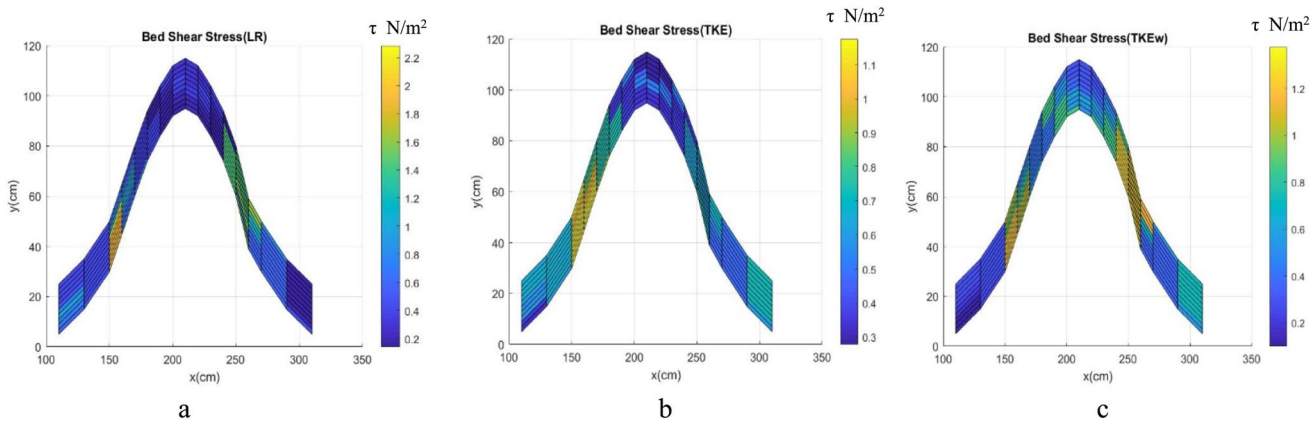

Fig. 10 Main channel bed shear stress distribution (**a**), linear regression (**b**), turbulent kinematic energy (**c**) and Modified Turbulent kinematic energy

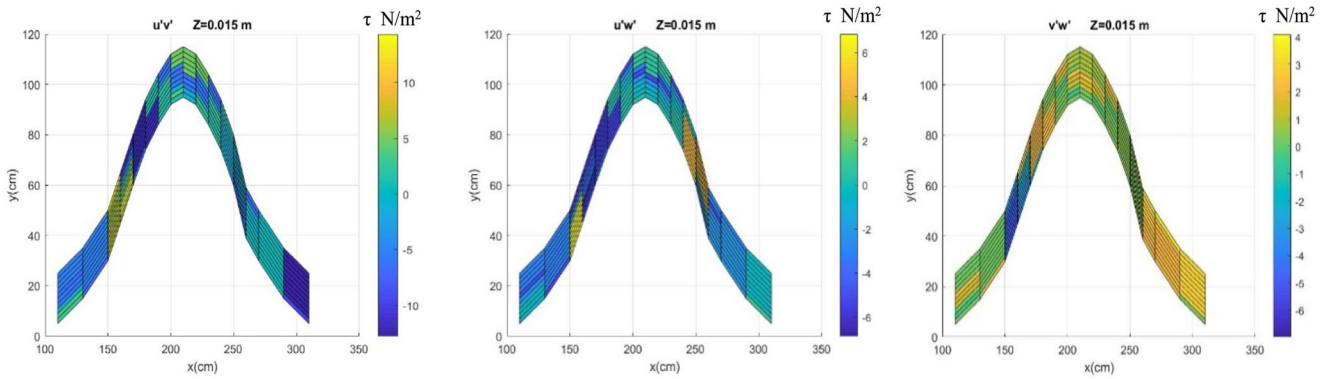

Fig. 11 Distribution of Reynolds shear stress in water relative depth 0.06

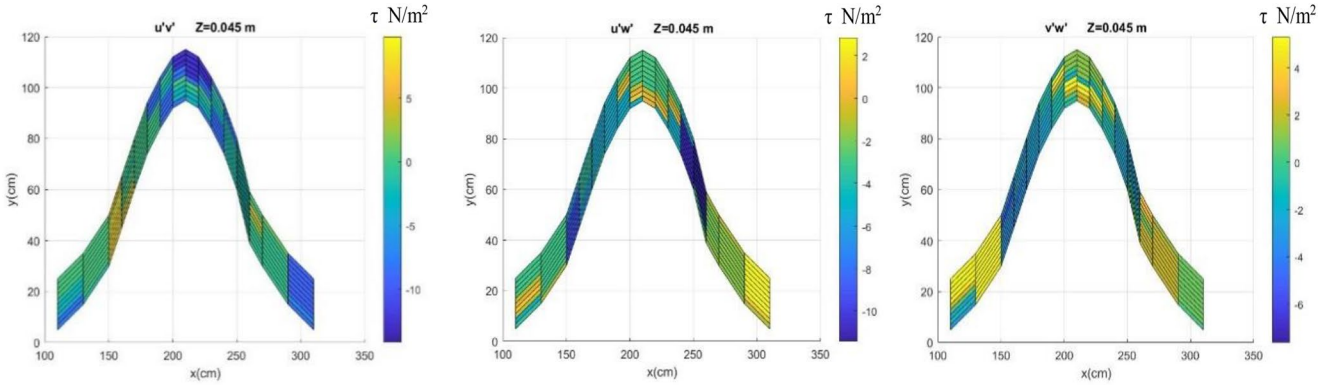

Fig. 12 Distribution of Reynolds shear stress in stress in water relative depth 0.18

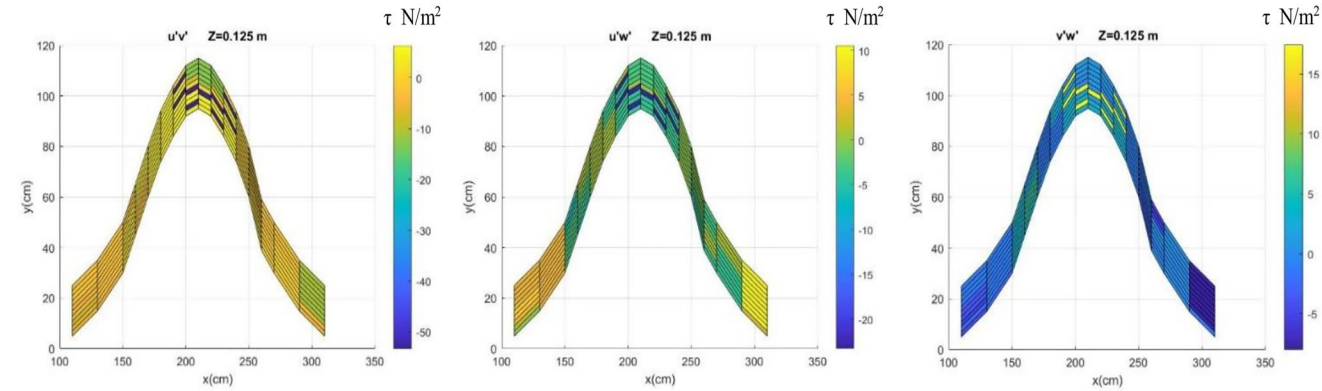

Fig. 13 Distribution of Reynolds shear stress in relative depth 0.5

Modifying of TKE and TKE-w′ methods

The re-estimation of TKE and TKE-w′ methods using the newly proposed constants, $\mathbf{c_1}$ and $\mathbf{c_2}$, from Zhang et al. (2020) and the present study is presented in Table 3. The results, evaluated based on error metrics such as RMSE and MAE, indicate a significant improvement in the accuracy of bed shear stress predictions, particularly for the TKE method. This finding suggests that specific constants may be necessary for precise shear stress estimation in meandering channel flows. Among the three bends analyzed, the lowest error values were observed in CS5 for both $\mathbf{c_1}$ and $\mathbf{c_2}$, indicating superior performance. Additionally, in other sections (CS1 and CS3), the newly proposed constants outperformed the

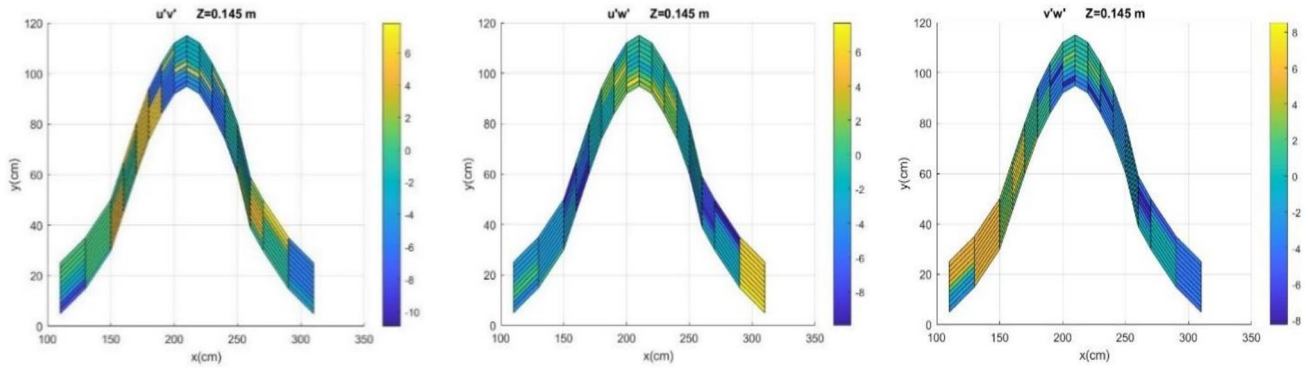

Fig. 14 Distribution of Reynolds shear stress in relative depth 0.58

conventional ones, as demonstrated by reduced statistical errors (RMSE and MAE).

Figure 15 compares shear stress values estimated by the TKE, TKE-w′, and RSM methods for CS1, CS3, and CS5, while Fig. 16 presents similar comparisons using the modified constants $\mathbf{c_1}$ and $\mathbf{c_2}$. These results demonstrate the impact of modifying the constants on improving the accuracy of shear stress predictions in compound meandering channels.

Comparison of shear stress methods

Figure 17 compares bed shear stress across five cross-sections, calculated using the previously described methods.

Table 3 C_1 and C_2 errors in CS_1, CS_3 and CS_5

				RMSE		*MAE*	
		c_1	c_2	TKE	TKE-W'	TKE	TKE-W'
Present research	CS_1	0.18	0.30	1.05	0.92	0.95	0.79
	CS_3	0.18	0.30	0.75	0.65	0.69	0.58
	CS_5	0.18	0.30	0.34	0.58	0.30	0.42
Kim et al. (2000)	CS_1	0.20	0.90	1.10	1.58	1.00	1.41
	CS_3	0.20	0.90	0.79	1.05	0.72	0.97
	CS_5	0.20	0.90	0.34	1.43	0.30	0.83
Zhang et al. (2020)	CS_1	0.23	0.44	1.18	1.06	1.08	0.93
	CS_3	0.23	0.44	0.84	0.74	0.77	0.67
	CS_5	0.23	0.44	1.07	0.70	0.42	0.46

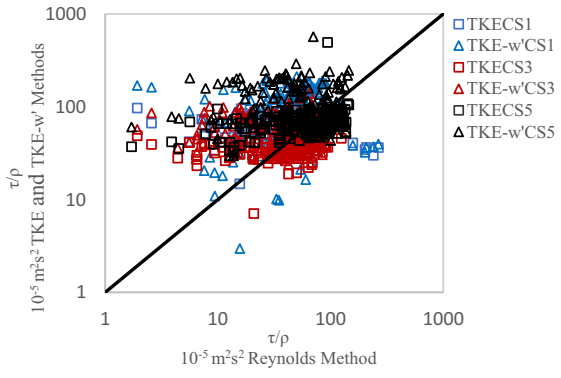

Fig. 15 Comparison of shear stress estimation between TKE, TKE-w′ and RSM methods in CS_1, CS_3 and CS_5

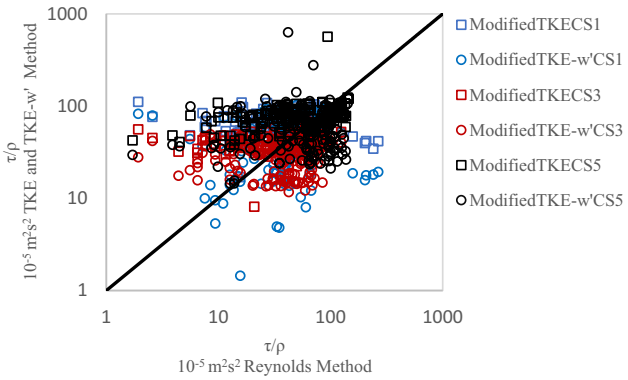

Fig. 16 Comparison of shear stress estimation between TKE, TKE-w′ and RSM methods in CS_1, CS_3 and CS_5 using new constants c_1 and c_2

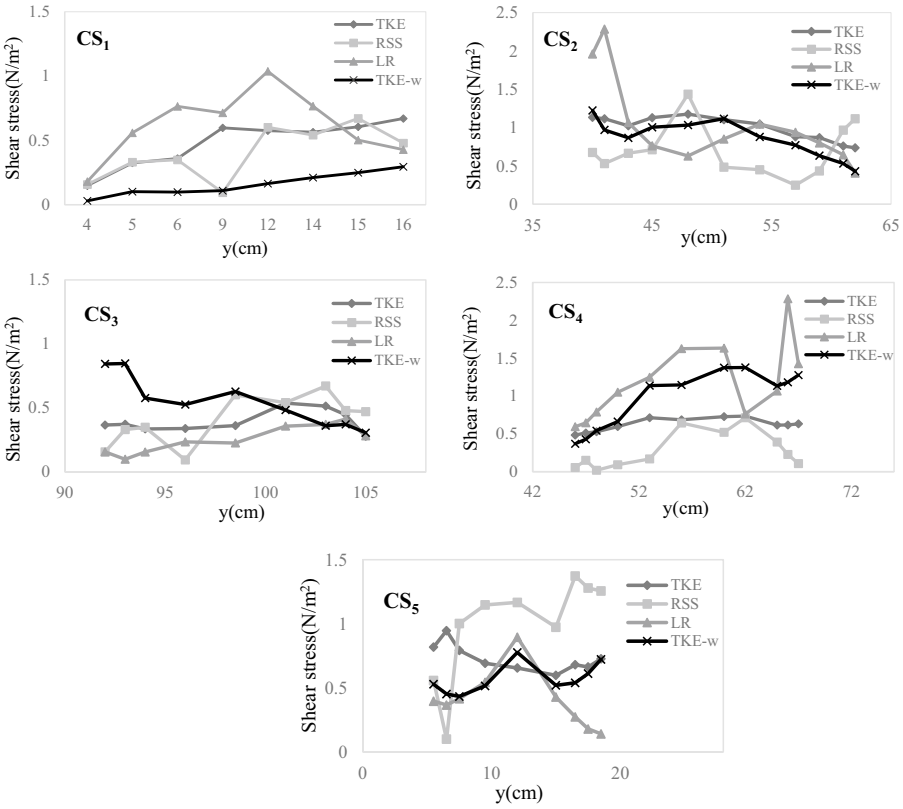

Fig. 17 Bed shear estimates turbulent kinetic energy (TKE), modified turbulent kinetic energy (TKE-w′), modified TKE, modified TKE-w′, linear regression (LR), and Reynolds shear stress extrapolation (RSS)

Table 4 The shear stress of flow relative depth at the middle axis of the main channel across different sections (N/m^2)

Methods	Relative depth	CS01	CS02	CS03	CS04	CS05
RSM	0.06	−0.67	0.45	−0.60	−0.52	−0.97
RSM	0.18	−0.14	0.08	−0.14	−0.06	−0.88
RSM	0.38	−0.11	−0.7	−0.63	0.89	−0.54
RSM	0.58	−0.36	−0.16	−0.41	0.09	−0.41
TKE	0.06	0.60	1.04	0.36	0.73	0.6
TKE	0.18	0.66	1.04	0.43	0.74	0.69
TKE	0.38	0.67	0.93	0.41	0.86	0.72
TKE	0.58	0.49	0.71	0.37	0.42	0.80
TKE-w′	0.06	0.25	0.88	0.63	1.37	0.52
TKE-w′	0.18	1.60	2.1	0.87	2.24	1.00
TKE-w′	0.38	1.52	1.74	0.61	1.82	1.33
TKE-w′	0.58	1.37	1.68	0.69	0.86	1.97
RS-TKE*	0.06	0.54	0.94	0.32	0.65	0.54
RS-TKE	0.18	0.70	0.93	0.39	0.66	0.62
RS-TKE	0.38	0.74	0.84	0.37	0.77	0.65
RS-TKE	0.58	0.52	0.64	0.33	0.38	0.72
RS-TKE-w′**	0.06	0.04	0.29	0.20	0.46	0.17
RS-TKE-w′	0.18	0.45	0.70	0.29	0.75	0.33
RS-TKE-w′	0.38	0.53	0.58	0.20	0.61	0.44
RS-TKE-w′	0.58	0.50	0.56	0.23	0.29	0.66

*Re-estimated turbulent kinetic energy (TKE)

**Re-estimated modified turbulent kinetic energy (TKE-w′)

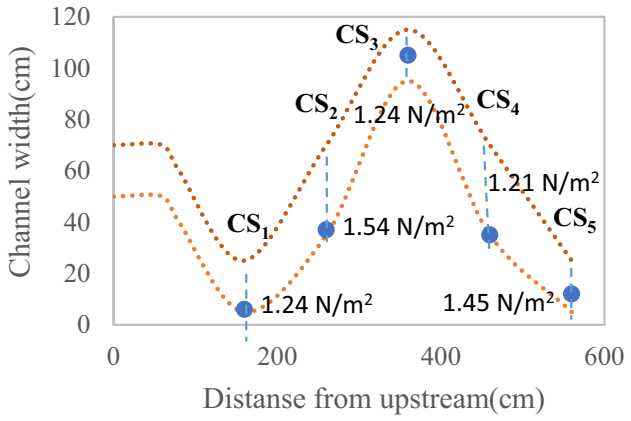

Fig. 18 Maximum shear stress location and quantities throughout channel length

Table 5 Locations and quantities of maximum shear stress

CS no	x (cm)	y (cm)	z (cm)	RSM (N/m^2)
CS_1	160	6	6.5	1.24
CS_2	260	37	12.5	1.54
CS_3	360	105	4.5	1.24
CS_4	460	35	18	1.21
CS_5	560	12	6.5	1.45

The results indicate that the maximum discrepancy among the methods occurs in the outer region, which is influenced by shear layers and secondary flows. The presence of the right-side wall appears to reduce shear stress values due to the interaction and exchange of momentum in this region. Notable irregularities in the shear stress distribution are observed, particularly in CS4 and CS5. The best agreement between the methods is observed at the second bend (CS3), likely due to the influence of walls and corner regions near the narrow floodplains and around the main channel. In CS2 and CS4, higher shear stress values highlight the significant role of the two floodplain areas in generating friction at the interfaces and facilitating momentum exchange. Table 4 presents the shear stress values relative to the flow depth along the middle axis of the main channel for the various cross-sections (in N/m^2).

Maximum shear stress

The stable design of channels requires a thorough understanding of maximum shear stresses. To examine the longitudinal variation in maximum shear stress, Fig. 18 is plotted based on the data in Table 5. This figure illustrates the locations of maximum shear stress along the channel length as well as the corresponding shear stress values at various cross-sections. The results reveal that, except for CS3, the maximum shear stress is consistently located near the outer bank, as noted by Tilson (2005). This finding suggests that these areas of flow in compound meandering channels are particularly susceptible to degradation (Hooke 1975; Lee et al. 2019). Additionally, Fig. 17 demonstrates that the shear stress at CS2 is higher than at CS4. This can be attributed to the inflow of water into the bend at CS2 occurring along the spanwise direction, which intensifies the momentum exchange and, consequently, the shear stress (Mera et al. 2015).

Conclusions

This study evaluated the accuracy of various methods for calculating shear stress in compound meandering channels. Data collected from the main channel of a physical meander model was used to assess four widely applied methods: linear regression of the flow velocity profile, turbulent kinetic energy (TKE), modified turbulent kinetic energy (TKE), and Reynolds shear stress extrapolation. Acoustic doppler velocimeter (ADV) data was analyzed to determine bed shear stress. The findings revealed that the maximum bed shear stress occurs at the entrance of the bend section (CS2). This observation suggests that the interaction between flow dynamics and channel geometry at the bend entrance (CS2) plays a significant role in sediment transport processes within meandering channels. To enhance the accuracy of shear stress calculations in these regions, the study explored the application of two modified TKE equations incorporating newly proposed constants (c_1 and c_2). These modifications significantly improved shear stress predictions compared to traditional methods. Additionally, the results demonstrated that the TKE and TKE-w' methods effectively predict shear stress distribution throughout the channel depth, even in the presence of complex three-dimensional turbulent flow patterns. The analysis identified five sections with the highest maximum shear stress, underscoring these areas as critical zones for sediment management in meandering river systems.

Author contribution Vahideh Mortazavi Amiri wrote the main manuscript text Kazem Esmaili reviewed the manuscript.

Data availability No datasets were generated or analysed during the current study.

Declarations

Conflict of interest The authors declare no competing interests.

References

Alfadhli I, Yang S & Sivakumar M (2013) Distribution of Reynolds shear stress in steady and unsteady flows. SGEM: 13th International

Multidisciplinary Scientific Geo conference, pp 109–116. Bulgaria: SGEM
Babaeyan-Koopaei K, Ervine DA, Carling PA, Cao Z (2002) Velocity and turbulence measurements for two overbank flow events in River Severn. J Hydraul Eng ASCE 128(10):891–900
Barahimi M, Sui J (2024) Deformation of vegetated channel bed under ice-covered flow conditions. J Hydrol. https://doi.org/10.1016/j.jhydrol.2024.131280
Bauri KP, Sarkar A (2018) Turbulent burst-sweep events around fully submerged vertical square cylinder over plane bed. Environ Fluid Mech 19:645666. https://doi.org/10.1007/s10652-018-9643-3
Bernard and Handler (1990) Reynolds stress and the physics of turbulent momentum transport. J Fluid Mech 220:99–124
Biron PM, Robson C, Lapointe MF, Gaskin SJ (2004) Comparing different methods of bed shear stress estimates in simple and complex flow fields. Earth Surf Proc Land 29:1403–1415
Blanckaert K (2011) Hydrodynamic processes in sharp meander bends and their morphological implications. J Geophys Res Earth Surf 116(F01003):10
Chen KH, Xia YF, Zhang SZ, Wen YC, Xu H (2018) Experimental research on boundary shear stress in typical meandering channel. China Ocean Eng 32(3):365–373. https://doi.org/10.1007/s13344-018-0038-5
Esfahani FS, Keshavarzi A (2011) Effect of different meander curvatures on spatial variation of coherent turbulent flow structure inside ingoing multi-bend river meanders. Stochastic Environ Res Risk Assess 25(7):913–928
Esfahani FS, Keshavarzi A (2020) Circulation cells topology and their effect on migration pattern of different multi-bend meandering rivers. Int J Sedim Res. https://doi.org/10.1016/j.ijsrc.2020.04.004
Ferreira Da Silva AM (2006) On why and how do rivers meander. J Hydraul Res 44(5):579–590
Guo J, Julien PY (2005) Shear stress in smooth rectangular open-channel flows. J Hydraul Eng 131(1):30–37
Hafez YI (2022) Excess energy theory for river curvature and meandering. J Hydrol. https://doi.org/10.1016/j.jhydrol.2022.127604
Hooke RLB (1975) Distribution of sediment transport and shear stress in a meander bend. J Geol 83(5):543–565
Hopkinson L, Wynn-Thompson T (2012) Streambank shear stress estimates using turbulent kinetic energy. J Hydraul Res 50(3):320–323
Imagbe LO (2021) Sediment grains entrainment: comparing bed shear stress estimation methods. J Geol Geophys 10(8):1001004
Ippen AT, Drinker PA (1962) Boundary shear stresses in curved trapezoidal channels. J Hydraul Div 88(5):143–180
Ippen AT, Drinker PA, Jobin WR and Noutsopoulos GK (1960) The distribution of boundary shear stresses in curved trapezoidal channels. Technical Report No. 43, Department of Civil and Sanitary Engineering, Massachusetts Institute of Technology
Jing H, Guo Y, Li C, Zhang J (2009) Three-dimensional numerical simulation of compound meandering open channel flow by Reynolds stress model. Int J Num Method Fluid 59:927–943
Keshavarzi AR, Gheisi AR (2006) Stochastic nature of three dimensional bursting events and sediment entrainment in vortexchamber. J Stoch Environ Res Risk Assess 21(1):75–87
Kim SC, Friedrichs CT, Maa JPY, Wright LD (2000) Estimating bottom stress in a tidal boundary layer from acoustic Doppler velocimeter data. J Hydraul Eng 126:399–406
Lee SK, Dang TA, Le VT (2019) Investigation of shear stress distribution in a 90-degree channel bend. Int J Appl Mech Eng 24(1):213–220
Mera I, Franca MJ, Anta J, Penta E (2015) Turbulence anisotropy in a compound meandering channel with different submergence conditions. Adv Water Resour 81:142–151
Mignot E, Harther D, Barthelemy E (2009) On the structure of shear stress and turbulent kinetic energy flux across the roughness layer of a gravel-bed channel flow. J Fluid Mech 638:423–452
Naghavi M, Mohammadi M, Mahtabi G (2023) The effect of building arrangement on the flow characteristics in meandering compound channels. J Environ Manage. https://doi.org/10.1016/j.jenvman.2023.117288
Noorbakhsh F, Parola AC (2018) Numerical investigation of the effect of river modelling parameters on bed shear stress. In: World Environmental and Water Resources Congress, pp 169–175
Omran M, Knight DW (2010) Modeling secondary cells and sediment transport in rectangular channels. J Hydraul Res 48(2):205–212
Pan Y, Li Z, Yang K, Jia D (2019) Velocity distribution characteristics in meandering compound channels with one-sided vegetated floodplains. J Hydrol 578:124068
Parsapour-Moghaddam P, Rennie CD (2017) Hydrostatic versus non-hydrostatic hydrodynamic modeling of secondary flow in a tortuously meandering river: application of Delft3D. River Res Appl 33(9):1400–1410
Rameshwaran P, Naden PS (2003) Three-dimensional numerical simulation of compound channel flows. J Hydraul Eng (ASCE) 129:645–652
Shan Y, Liu C, Luo M (2015) Simple analytical model for depth-averaged velocity in meandering compound channels. Appl Math Mech 36(6):707–718
Sin K (2010) Methodology for calculating shear stress in a meandering channel. Diss. Colorado State University
Soulsby RL (1983) The bottom boundary layer of shelf seas. In: Johns B (ed) Physical oceanography of coastal and shelf seas. 189–266
Stapleton K, Huntley D (1995) Seabed stress determinations using the inertial dissipation method and the turbulent kinetic energy method. Earth Surf Process Landforms 20(9):807–815
Tilston M (2005) Three-dimensional flow structure, turbulence and bank erosion in a 180° meander loop. Thesis, University of Montreal, Quebec, Canada
Uchida T, Fukuoka S (2014) Numerical calculation for bed variation in compound-meandering channel using depth integrated model without assumption of shallow water flow. Adv Water Resour 72:45–56
Ursic M, Thornton C, Cox A and Abt S (2012) Quantification of shear stress in a meandering native topographic channel using a physical hydraulic model, Technical Report, Engineering Research Centre Fort Collins, Colorado
Wahl TL (2000) Analysing ADV data using WinADV. 2000 Joint conference on water resources engineering and water resources planning & management July 30–August 2, 2000 – Minneapolis, Minnesota
Yang SQ, Lee JW (2007) Reynolds shear stress distributions in a gradually varied flow in a roughened channel. J Hydraul Res 45(4):462–547
Yang SQ, McCorquodale JA (2004) Determination of boundary shear stress and Reynolds shear stress in smooth rectangular channel flows. J Hydraul Eng 130:458–462
Zarrati AR, Jin Y, Karimpour S (2008) Semi-analytical model for shear stress distribution in simple and compound open channels. J Hydraul Eng 134(2):205–215
Zhang L, Zhang F, Cai A, Song Z, Tong S (2020) Comparison of methods for bed shear stress estimation in complex flow field of bend. Water 12(10):2753